Batteries & Supercaps

Research Article
doi.org/10.1002/batt.202400034

Chemistry Europe
European Chemical Societies Publishing

www.batteries-supercaps.org

Pairing Non-Solvating Cosolvent with Weakly Solvating Solvents for Facile Desolvation to Enable EC-Free and High-Rate Electrolyte for Lithium Ion Batteries

Qijun Liu,[a, b] Ziqi Zeng,*[a] Mingsheng Qin,[a, b] Tao Yang,[c] Hongyun Ma,[d] Sheng Ji,[c] Ling Huang,[d] Shijie Cheng,[a] and Jia Xie*[a]

The advancement of lithium-ion batteries (LIBs) calls for superior electrolyte design to satisfy the booming demands of energy storage markets. Despite being typically indispensable in modern electrolytes, ethylene carbonate (EC) exhibits strong affinity with Li^+ and derives organic-rich SEI, leading to sluggish interfacial dynamics and unsatisfied rate capability. Here, we construct a kinetically favorable electrolyte based on linear carbonates (DMC) and fluoroethylene carbonate (FEC) with functional non-solvating cosolvent, fluorobenzene (FB). Specifically, DMC and FEC, as weak binding solvents, show facile interfacial kinetics. FB enables a loose coordination chemistry through dipole-dipole interaction, further lubricating Li^+ desolvation and transport through SEI at interphase, which accelerates electrochemical kinetics and enables improved rate performance (257 $mA\,h\,g^{-1}$ is achieved for graphite at 6 C). Moreover, the optimized electrolyte shows decent graphite compatibility, long-term stability (75% capacity retention after 350 cycles for NCM622/graphite pouch cells at 1 C) and wide-temperature adaptability (−40~160 °C). This work reveals that dipole-dipole interaction between non-solvating cosolvents and solvents can effectively lower desolvation energy barrier and ultimately enable good rate capability, which provides a new avenue for designing EC-free electrolyte in high-rate LIBs.

Introduction

Lithium-ion batteries (LIBs) are widely deployed in modern society, including portable electronics, electric vehicles (EVs) and large-scale energy storage,[1–6] which calls for superior LIBs featuring high rate capability, long-term stability and wide temperature adaptability simultaneously.[7–10] So far, commercial LIBs heavily rely on ethylene carbonate (EC)-based electrolytes due to their decent Li salts' dissociation and interfacial passivation.[11,12] Nevertheless, despite the high ionic conductivity of EC-based electrolytes (> 10 $mS\,cm^{-1}$) at room temperature, graphite anode faces slothful interfacial kinetics, contributing to unsatisfied high rate performance of LIBs[13] Consequently, issues such as lithium plating and rapid capacity decay manifest at high rate.[14] This limitation arises from the solid electrolyte interphase (SEI) with high Li^+ diffusion resistance and sluggish desolvation kinetic at the interphase (desolvation energy barrier ~50–70 $kJ\,mol^{-1}$).[15–17] Additionally, the high-melting point of EC (36.4 °C) hinders low-temperature performance of LIBs,[18] where desolvation process becomes even more energy-consuming at the same time.[19,20] As a result, it's imperative to develop EC-free electrolyte with tunable Li^+-solvent affinity and accelerated interfacial kinetic for superior LIBs.

Recently, high concentration electrolytes (HCEs)[21] and localized HCEs[22] have been developed to improve rate performance by increasing lithium salts' concentration. Specifically, the inorganic-rich SEI derived from this anion-engaged environment exhibits low Li^+ diffusion resistance.[23] More importantly, the entrance of anions into Li^+ solvation shell also weakens the Li^+-solvents strength, enabling enhanced desolvation kinetics.[24,25] Nevertheless, challenges still remain as demonstrated by its high cost and relatively low ionic conductivity (< 5 $mS\,cm^{-1}$).[26] Weakly solvating electrolyte (WSE), featuring weak coordination ability and anion-rich solvation shell, is another effective strategy to improve the rate performance of LIBs. However, most of WSE based on ether solvents (e.g. dimethoxymethane, 1,4-dioxane) still suffers from insufficient oxidation stability and low ionic conductivity.[27,28] Fortunately, linear ester (DMC) featuring moderate solvating capability and wide electrochemical window holds great promise to design high-rate electrolyte. Besides, halogenated aromatic hydrocarbons (e.g., fluorobenzene, trifluoro-benzene)

[a] Q. Liu, Dr. Z. Zeng, M. Qin, Prof. S. Cheng, Prof. J. Xie
State Key Laboratory of Advanced Electromagnetic Engineering and Technology, School of Electrical and Electronic Engineering
Huazhong University of Science and Technology
Wuhan 430074, Hubei (China)
E-mail: ziqizeng@hust.edu.cn
xiejia@hust.edu.cn

[b] Q. Liu, M. Qin
State Key Laboratory of Materials Processing and Die & Mould Technology, School of Materials Science and Engineering
Huazhong University of Science and Technology
Wuhan 430074, Hubei (China)

[c] T. Yang, S. Ji
Jiangsu Chunlan Clean Energy Research Institute Co., Ltd
Taizhou 225300, Jiangsu (China)

[d] H. Ma, L. Huang
Tianjin Lishen Battery Joint-Stock Co., Ltd
Tianjin 300384, China

Supporting information for this article is available on the WWW under https://doi.org/10.1002/batt.202400034

Research Article
doi.org/10.1002/batt.202400034
Chemistry Europe
European Chemical Societies Publishing

allows for further fine tuning Li^+-solvent affinity based on dipole-dipole interaction, thus facilitating desolvation.[29–32] These results inspire us to pair non-solvating cosolvent with weakly solvating solvents to tune Li^+-solvent binding strength, which might facilitate interfacial desolvation and improve rate performance.

In this work, we use the E_{min} value of ESP to provide a straightforward description of the solvent's capacity to bind with Li^+. Firstly, we replace EC solvent by weak binding solvents (fluoroethylene carbonate (FEC) and dimethyl carbonate(DMC)), constructing a weakly solvating structure. To further improve interfacial kinetics, we use fluorobenzene (FB) as cosolvent to accelerate desolvation at electrode/electrolyte interphase, which exerts dipole-dipole interaction to construct a loose Li^+ solvation (Figures 1a, b). Based on this principle, we develop an EC-free electrolyte composed of LiFSI: FEC: DMC: FB = 1: 1: 4: 3 (by molar ratio) (denoted as L1F4D3FB). It is found that the addition of FB accelerates desolvation at electrode/electrolyte interphase without altering Li^+ solvation structure, contributing to fast interfacial kinetics and excellent rate performance of graphite anode. As a result, the L1F4D3FB enables the graphite/Li cells to achieve better rate capability (257 mA h g^{-1} at 6 C) than traditional carbonate electrolyte (only 25.2 mA h g^{-1} at 6 C). Besides, the practicality of L1F4D3FB is also demonstrated in NCM622/graphite pouch cells. Furthermore, we provide a simple and feasible principle that (i) an intrinsically loose solvation structure is constructed with weakly solvating solvent and (ii) functional cosolvents are introduced to weaken the Li^+-solvents strength, which results in lowered desolvation energy barrier and improved rate performance.

Results and Discussion

Rational Design of EC-Free Electrolyte

DMC is a commonly adopted linear carbonate featuring good graphite compatibility, low viscosity and acceptable Li salts' dissociation capability.[33] Moreover, the modest dipole moment of DMC suggests reduced ion-dipole interaction, particularly in comparison to the strong polar solvents (EC, PC). Our previous work shows that the incorporation of FB into electrolyte with moderate Li salts' concentration leads to notably electrochemical performance improvement.[29] Thus, LiFSI: DMC in a 1 : 5 molar ratio (designated as L5D) is chosen as a paradigm to demonstrate the effectiveness of FB for further lubricating desolvation. Besides, FEC is added into L5D to construct a low barrier and stable interphase (referred to as L1F4D),[34] and at the same time, its solvating ability is weaker than that of EC because of the electron-withdrawing effect of F atom. Note that the introduction of FEC results in negligible improvement in ionic conductivity (Figure S1a). Subsequently, FB is added into L1F4D (ionic conductivity of 7.72 mS cm^{-1}), showing an enhanced ionic conductivity for L1F4D1FB (8.74 mS cm^{-1}) since its reduced viscosity. However, excessive FB (L1F4D7FB) contributes to inferior ionic conductivity (4.25 mS cm^{-1}) because of the decreased Li^+ concentration in electrolyte (Figure S1b). Then,

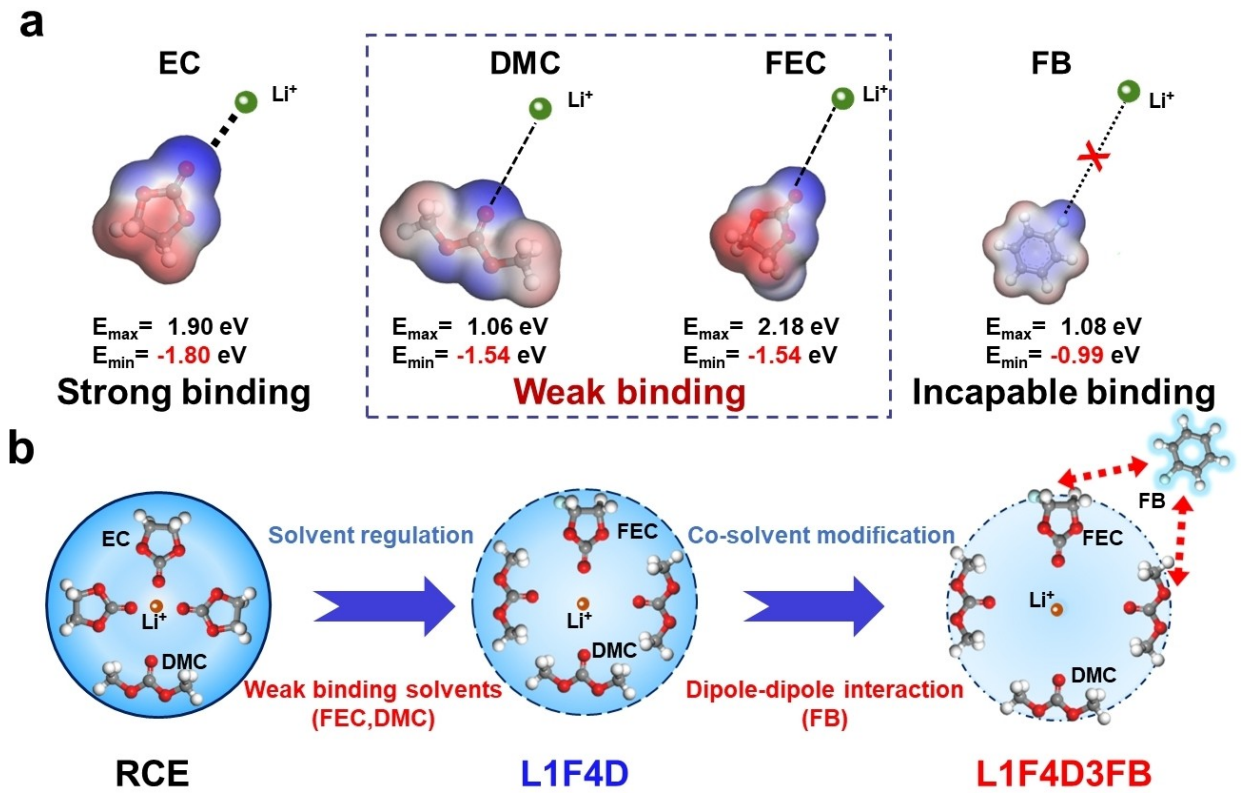

Figure 1. (a) The electrostatic potential (ESP) results of EC, DMC, FEC and FB. (b) The illustrations for solvation structure of RCE, L1F4D and L1F4D3FB.

Research Article
doi.org/10.1002/batt.202400034
Chemistry Europe
European Chemical Societies Publishing

graphite/Li half cells were studied in various electrolytes to find the optimal content of FB, in which L1F4D3FB affords the best rate performance (Figure S1c). As a result, L1F4D3FB is selected as a paradigm for subsequent investigations and the mechanism for improved rate performance is discussed latter despite its moderate ionic conductivity of 5.54 mS cm^{-1}.

Electrochemical Performance

Cyclic voltammetry was performed to study the electrochemical process. As displayed in Figure 2a, the graphite/Li cell in traditional carbonate electrolyte (1 M $LiPF_6$ in EC/DMC 1 : 1 vol%, denoted as RCE) shows high polarization, indicating relatively sluggish electrochemical dynamics. The cell in L5D exhibits an irreversible peak at 0.6 V, which signifies the irreversible capacity at initial stage. As for L4D1F, this peak (0.6 V, vs. Li/Li$^+$) disappears, indicating enhanced reversibility after adding FEC. Note that, the cell in L1F4D3FB shows overlapping patterns and the low polarization, suggesting good reversibility and favorable electrochemical kinetics (Figure 2a and Figure S2). The electrochemical performance was assessed in varied electrolytes within 2.0 and 0.01 V using graphite/Li cells. As illustrated in Figure 2b, the irreversible decomposition of L5D results in a low initial Coulombic efficiency (ICE, 84.5%), which is comparable to that of L4D1F (84.7%). Note that the cell in L1F4D3FB shows even lower ICE (83.4%), which is caused by the decomposition of FB to form SEI. As a result, the reliable interfacial passivation in L1F4D3FB enables the highest reversible capacity and stable Coulombic efficiency (CE > 99%) during following cycling. The rate capability of graphite/Li cells in different electrolytes is compared. The cell using L1F4D3FB achieves a high specific capacity of 257 mA h g^{-1} at 6 C, which is superior to others. A similarly poor rate performance is obtained in RCE regardless of Li salts (LiFSI and $LiPF_6$), indicating the solvent-related limitations (e.g., EC and DMC) rather the anions-induced restrains (e.g., FSI^- and PF_6^-) at high rate. (Figures 2c, d). Moreover, the cycling stability of cells using L5D and RCE decrease sharply after rate tests, suggesting the damaged interphase caused by current fluctuations (Figure S3). The long-term cycling stability is shown in Figure 2e. The cell in L5D suffers from rapid capacity decay over 100 cycles, suggesting

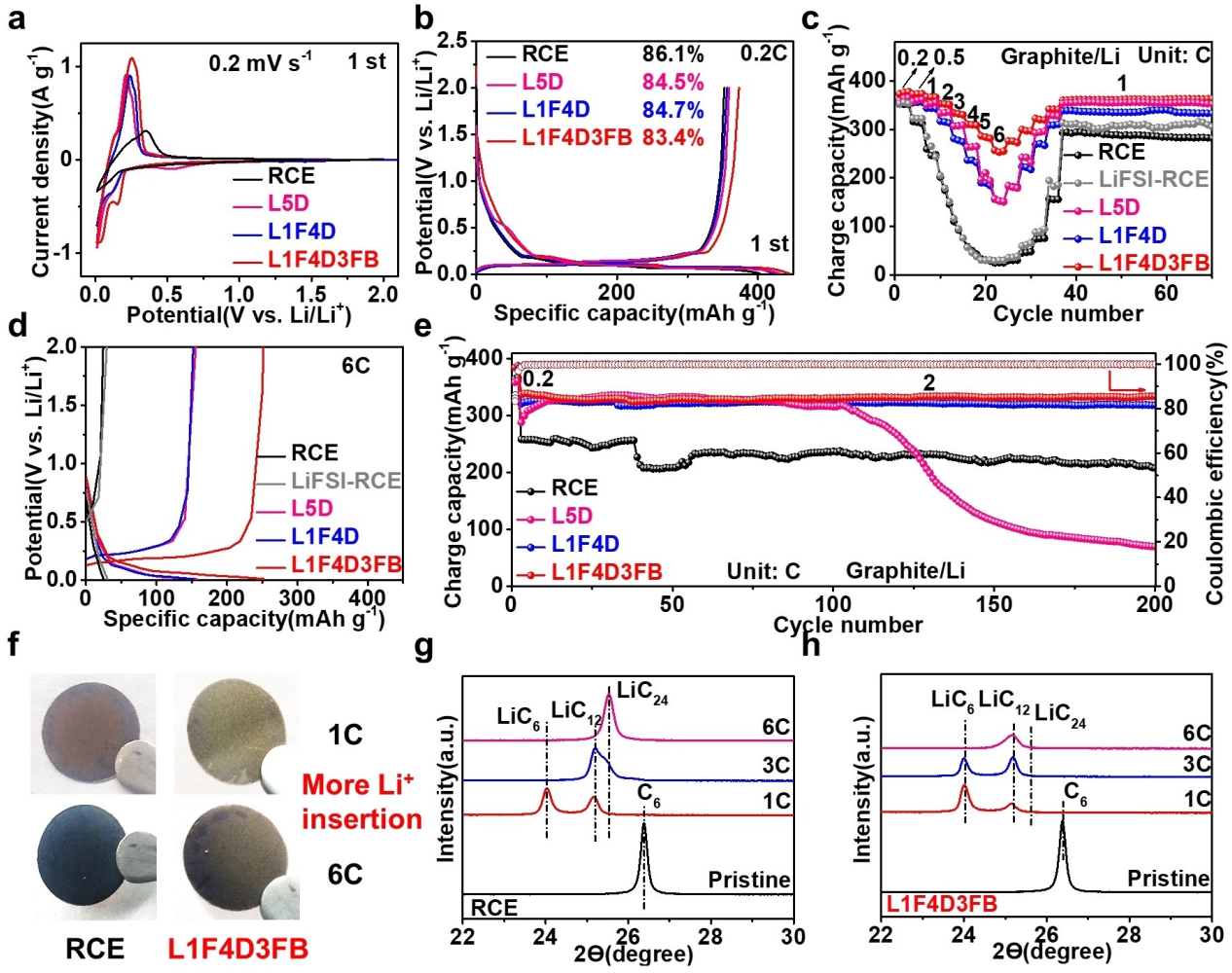

Figure 2. Electrochemical performance of different electrolytes. (a) CV curves, (b) initial charge-discharge curves, (c) rate capability, (d) charge-discharge curves of graphite/Li cells in different electrolytes at 6 C. (e) The long-term stability of graphite/Li cells in varied electrolytes. (f) Photographs of lithiated graphite anodes in varied electrolytes. XRD patterns of lithiated graphite anodes in (g) RCE, (h) L1F4D3FB at different charge rates.

poor interfacial compatibility and inferior reversibility. After the introduction of FEC, the cell shows improved cycling stability but still goes through unsatisfied rate performance (Figure 2c), highlighting the FEC-derived interfacial passivation for long-term stability. Furthermore, the L1F4D3FB affords stable cycling and improved rate capability simultaneously, indicating the reliable interfacial passivation and enhanced electrochemical kinetics. Although RCE enables graphite with stable cycling at 2 C, the specific capacity is merely 200 mA h g^{-1}. Correspondingly, the EC solvents in RCE strongly coordinate with Li^+ and form high resistance SEI, hindering interfacial kinetics process, leading to increased polarization and limited capacity (Figure 2a).

The digital photographs and XRD patterns of discharged graphite were acquired to investigate the rate capability. The graphite discharged in RCE shows dark red color at 1 C, indicating the formation of LiC_{12}, while the graphite in L1F4D3FB presents golden color, indicating the abundance of LiC_6 phase (Figure 2f).[35] Correspondingly, the prominent LiC_6 peak and a relatively weaker LiC_{12} peak are found in L1F4D3FB, revealing the high lithiation degree of the graphite (Figures 2g, h).[36,37] More importantly, as the rate increases, the peak assigned to LiC_{12} entirely vanishes at 3 C and the LiC_{24} peak located at 25.6° appears at 6 C in RCE (Figure 2g, h). Such change is also confirmed by the graphite's color. The sample employed RCE is dark black while the one utilizing L1F4D3FB appears pale yellow, which means the higher lithiation level in L1F4D3FB at high rate (Figure 2f),[38,39] Moreover, the Li–Li symmetric cells were operated with diverse electrolytes at 1 mA h cm^{-2} to confirm whether the superior performance achieved in graphite/Li cell results from the good compatibility of electrolyte with lithium metals. The Li/Li symmetric cells in three electrolytes exhibit severe voltage polarization (Figure S4), indicating the limited compatibility between the electrolyte and Li metal. The result is a side by side demonstration of the excellent adaptation between L1F4D3FB and graphite anode.

Solvation Structure

FB cannot dissolve lithium salt but keeps mixable with carbonates (e.g., DMC and FEC), hinting the possible molecular interaction between FB and carbonates. For this reason, Raman and NMR spectra were employed to study the FB-tuned Li^+-solvent interaction within bulk electrolyte. After Li^+ coordination (Figures 3a, b), the stretching vibration of C=O in DMC and FEC shows blue shift. However, a red shift is observed once FB is added, indicating the weakened Li^+-solvent interaction. Moreover, the peak intensity of Li^+-DMC is weakened upon adding FB (from 51% to 42%) (Figure 3c), further demonstrating the partially crippled Li^+-DMC binding in solvation shell. The similar weakened intensity can be observed for Li^+-FEC binding upon adding FB (Figure 3d).

In NMR results, the ^{7}Li signal shifts from −0.21 to −0.23 ppm after replacing a portion of DMC with FEC, suggesting the accumulation of electron cloud near Li^+ because of the stronger coulombic attractions between FEC and Li^+. The introduction of FB into the L1F4D results in a further upshift to −0.25 ppm, suggesting the additional accumulation of electron cloud around Li^+. Combined with the previous conclusion of weakened Li^+-solvent binding, the result demonstrates the strengthening of Li^+-FSI^- pairs (Figure 3e). Besides, the variation of ^{1}H signals for DMC, which moves from 3.82 to 3.79 ppm after the introduction of FB, suggests increased electron density around solvents due to the dipole-dipole interaction of FB–DMC (Figure 3f). The similar behavior that the ^{1}H signals upshift is observed in FEC upon adding FB (Figure S5). As a result, due to the existence of this highly electronegative F atom, the inherent dipole moment of FB attracts polar solvents (FEC and DMC), resulting in the weaker Coulombic force between Li^+ and the solvents but enhanced Coulombic force between Li^+ and anions. The weakened Li^+-solvent binding can accelerate the desolvation process, while the inorganic rich SEI produced by anions decomposition might speed up the transport of Li^+ through SEI, thus showing excellent intercalation kinetics of Li^+.

Based on above discussion, the introduction of FB can bring dipole-dipole interaction to weaken the coordination strength of Li^+-solvents (Figure 3g). The solvation structure for L1F4D and L1F4D3FB are illustrated in Figures 3h, i. In the former, strong Coulombic attractions tightly bond Li^+ and solvents in the solvation shell, leading to hampered desolvation. In contrast, the introduction of FB weakens Li^+-solvent strength, resulting in loosened solvation shell while maintaining original coordination chemistry, facilitating desolvation process in graphite anode, leading to enhanced rate capability.

Interfacial Behavior

To understand the origin of the improved rate capacity and excellent cycling stability in L1F4D3FB, the interfacial chemistry on cycled graphite was investigated by XRD, XPS, SEM and EIS. Figure S6 shows the XRD patterns of graphite cycled in varied electrolytes. The highest intensity of (002) diffraction peak is observed in L1F4D3FB, indicating well maintained graphite structure. To better understand the interfacial behavior, we analyze the chemical composition of SEI on cycled graphite. As shown in Figure 4a, a higher content of F is observed on graphite surface in L1F4D3FB, which derives from the decomposition of FEC, FB and anions. In addition, L1F4D3FB exhibits a lower content of O compared to L1F4D, which means the inhibited solvent decomposition. Figure 4a shows that a higher content of N and S is observed on graphite surface after the introduction of FB, which derives from the decomposition of FSI^-. The result confirms that the solvation structure contains more anions. In C 1s spectra, for above two electrolytes, the content of C–C/C–H, C–O and Li_2CO_3 peaks are similar, while the slightly higher C=O content obtained in L1F4D is contributed to the severe solvents' decomposition (Figure 4b and Figure S7). More importantly, the SEI contains even more LiF in L1F4D3FB after introducing FB, which is originated from FB and FEC (Figure 4c). In addition, N and S signals are intensified in L1F4D3FB compared to the L1F4D, indicating the preponderant decomposition of FSI^- anions in the solvation

Research Article
doi.org/10.1002/batt.202400034
Chemistry Europe
European Chemical Societies Publishing

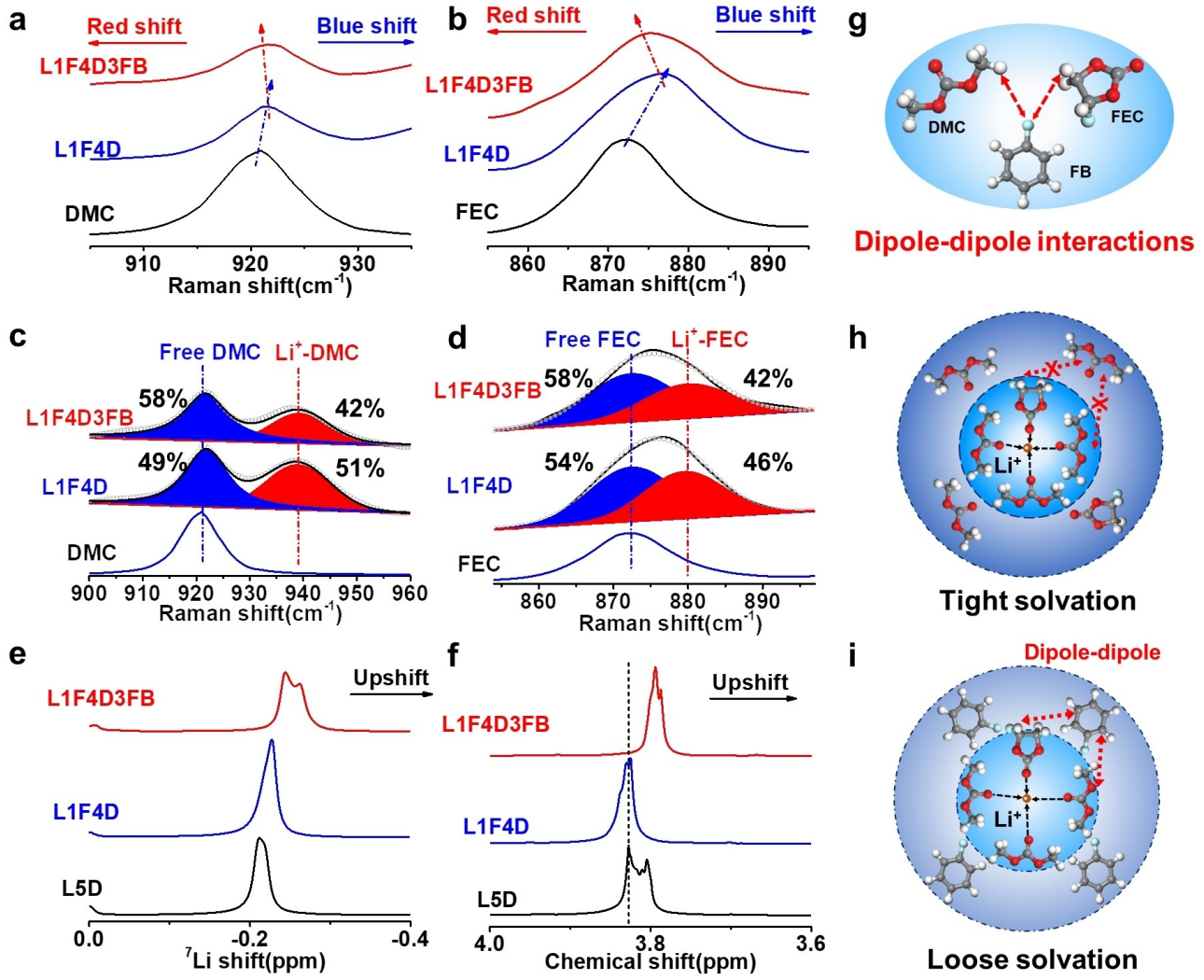

Figure 3. Experimental studies on solvation structures of varied electrolytes. Raman spectra of pure DMC and FEC, L1F4D and L1F4D3FB. Vibrations for (a) DMC and (b) FEC solvents. The fitted curves of (c) DMC and (d) FEC solvents. (e) ^{7}Li NMR (f) ^{1}H NMR results for different electrolytes. (g) Dipole-dipole interaction between FB and solvents. Schematic diagram of solvation shell for (h) L1F4D and (i) L1F4D3FB.

shell (Figure S8), which is consistent with the reality that anions' participation into solvation structure. In F 1s spectra, a dominant peak of $Li_xPO_yF_z$ is observed for graphite in RCE since the incomplete decomposition of $LiPF_6$ (Figure S9). Benefiting from the synergistic film-forming effect of FB, FEC and anions, the SEI derived from L1F4D3FB contains more inorganic components, inhibiting side reactions and accelerating Li^+ transfer, which enables stable long-term cycling performance and high rate capability.

Moreover, the graphite cycled in RCE and L5D shows rough surface (Figures 4d, e), indicating the continuous side reactions, which is consistent with the poor cycling performance. After adding FEC, the graphite surface is well maintained in certain degrees (Figure 4f). Benefiting from the excellent film formation of FB and FEC, the cycled graphite keeps smooth surface and structural integrity in L1F4D3FB (Figure 4g). The impedance of the interface is further investigated. As expected, the impedance of all cells decreases after activation process, indicating the formation of a SEI (Figures 4h, i and Figure S10). However, the cell resistance before and after cycling is significantly the highest in RCE, suggesting the unstable interface on graphite anodes (Figure 4j). In comparison, L1F4D3FB exhibits lower resistance SEI in the early stage and after high rate cycling. The results suggest that FEC and FB ensure the formation of a stable SEI with low impedance on graphite, which contributes to cycling stability and rate capability.

Electrode/Electrolyte Interface Kinetics

To understand the electrode/electrolyte interface kinetics, we employed temperature-dependent electrochemical impedance spectroscopy (EIS) to investigate two important parameters on graphite symmetry batteries: the activation energy for charge transfer resistance ($E_{a,ct}$) and Li^+ transport through SEI ($E_{a,SEI}$)[40] (Table S1). The resistance increases as the temperature drops (Figure S11), indicating the temperature-dependent electrochemical kinetics. As shown in Figure 5a, the activation energy

Research Article
doi.org/10.1002/batt.202400034
Chemistry Europe
European Chemical Societies Publishing

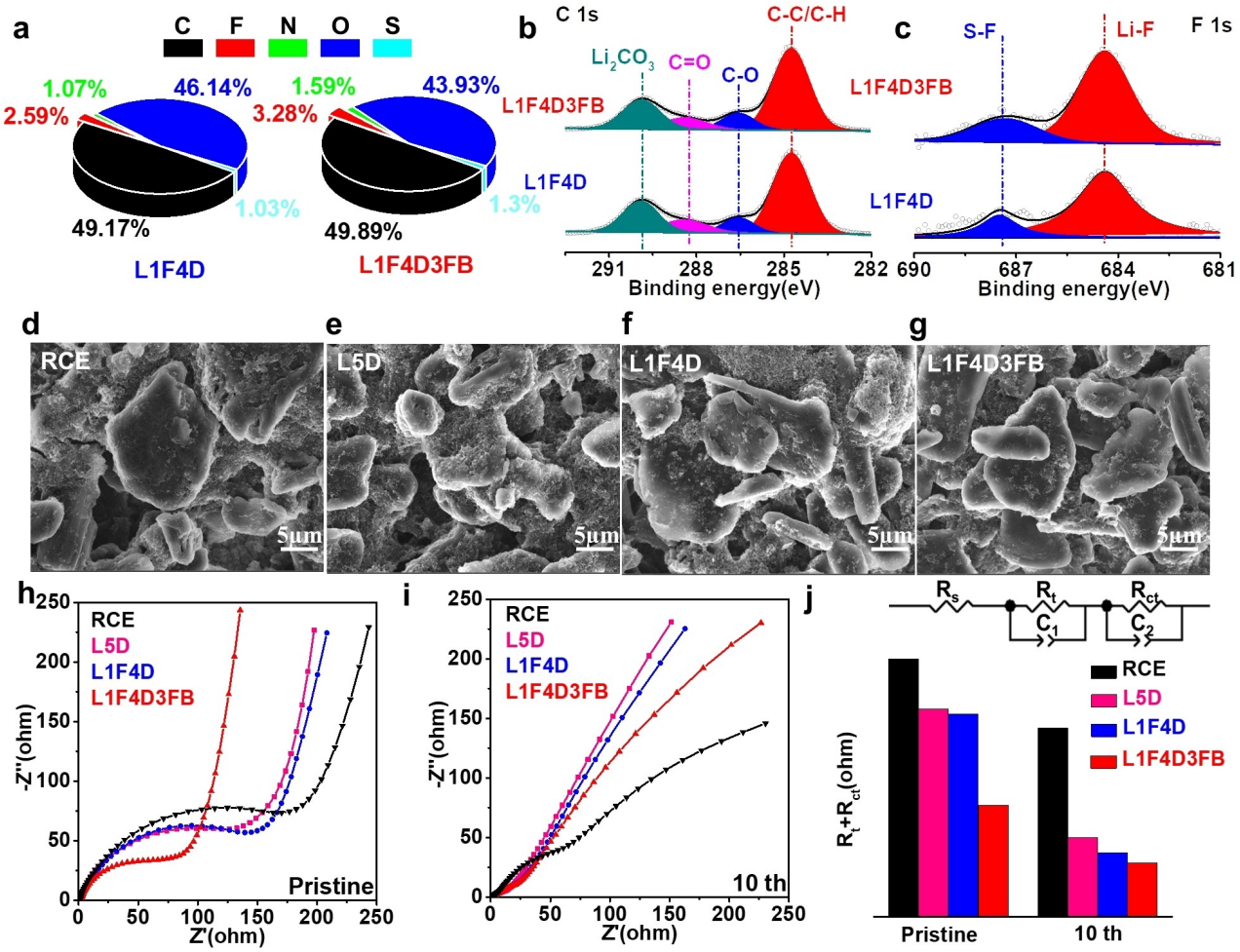

Figure 4. Interfacial chemistry of cycled graphite. (a) Elemental contents detected on graphite surface for L1F4D and L1F4D3FB. XPS results for (b) C and (c) F spectra. SEM images of graphite cycled in (d) RCE (e) L5D (f) L1F4D (g) L1F4D3FB. Nyquist curve for graphite at (h) pristine and (i) 10th. (j) The interfacial resistance derived from EIS results.

for charge transfer, relating to desolvation process, is calculated to be 0.61 eV in L1F4D, which is lower than that of RCE (0.64 eV) because of the displacement of strong-solvating EC by weak-solvating solvents (e.g., FEC and DMC). The introduction of FB results in a further reduction of $E_{a,ct}$ value to 0.55 eV, which is attributed to the FB-weakened Li^+-solvent binding and loose coordination. On the other hand, the $E_{a,SEI}$ value, representing the barrier for Li^+ transport through SEI, exhibits a decrease from 0.37 eV to 0.35 eV for L1F4D compared to RCE (Figure 5b). This reduction can be attributed to the LiF-rich and low-barrier SEI after FEC modification in L5D. Interestingly, the L1F4D3FB shows the lowest $E_{a,SEI}$ value (0.28 eV) since the inorganic-rich SEI originating from the decomposition of both FEC and FB. We further replace $LiPF_6$ with LiFSI to exclude the effect of anions on the activation energy. As expected, the replacement of lithium salts exhibits small change in activation energy (Figure 5a, b), indicating the rationalization of solvents is more important than anions in this scenario. The lowest $E_{a,ct}$ and $E_{a,SEI}$ indicate facilitated desolvation in L1F4D3FB, sustaining high rate performance in LIBs. In addition, the multistep CV is employed to understand ionic diffusion coefficient in LIBs.[41] As shown in Figure S12, the peak current increases as increasing sweep rates. A narrower peak separation and the highest slope (1.10) are observed in L1F4D3FB, suggesting efficient electrochemical kinetics in L1F4D3FB (Figure 5c).

Based on above discussion, the beneficial effect of FB in L1F4D3FB is schematically illustrated in Figure 5d. L1F4D3FB exhibits a loosened solvation shell since the weak Li^+-solvents binding and FB-modified Li^+-solvent-anions interaction in L1F4D3FB. The weakened Li^+-solvent coordination makes it easier for stripping off the solvation sheath, leading to lower activation energy of Li^+ desolvation. In contrast, a tight solvation shell is observed in RCE (Figure 5e), showing sluggish interfacial kinetics and inferior rate capability despite with higher bulk ionic conductivity. In addition, the decomposition of FEC and FB boosts inorganic content of SEI, resulting in faster Li^+ transport through SEI. The ultimate outcome is that lower $E_{a,ct}$ and $E_{a,SEI}$ indicate fast kinetics in Li^+ transport, conferring high rate capability in LIBs.

Research Article
doi.org/10.1002/batt.202400034
Chemistry Europe
European Chemical Societies Publishing

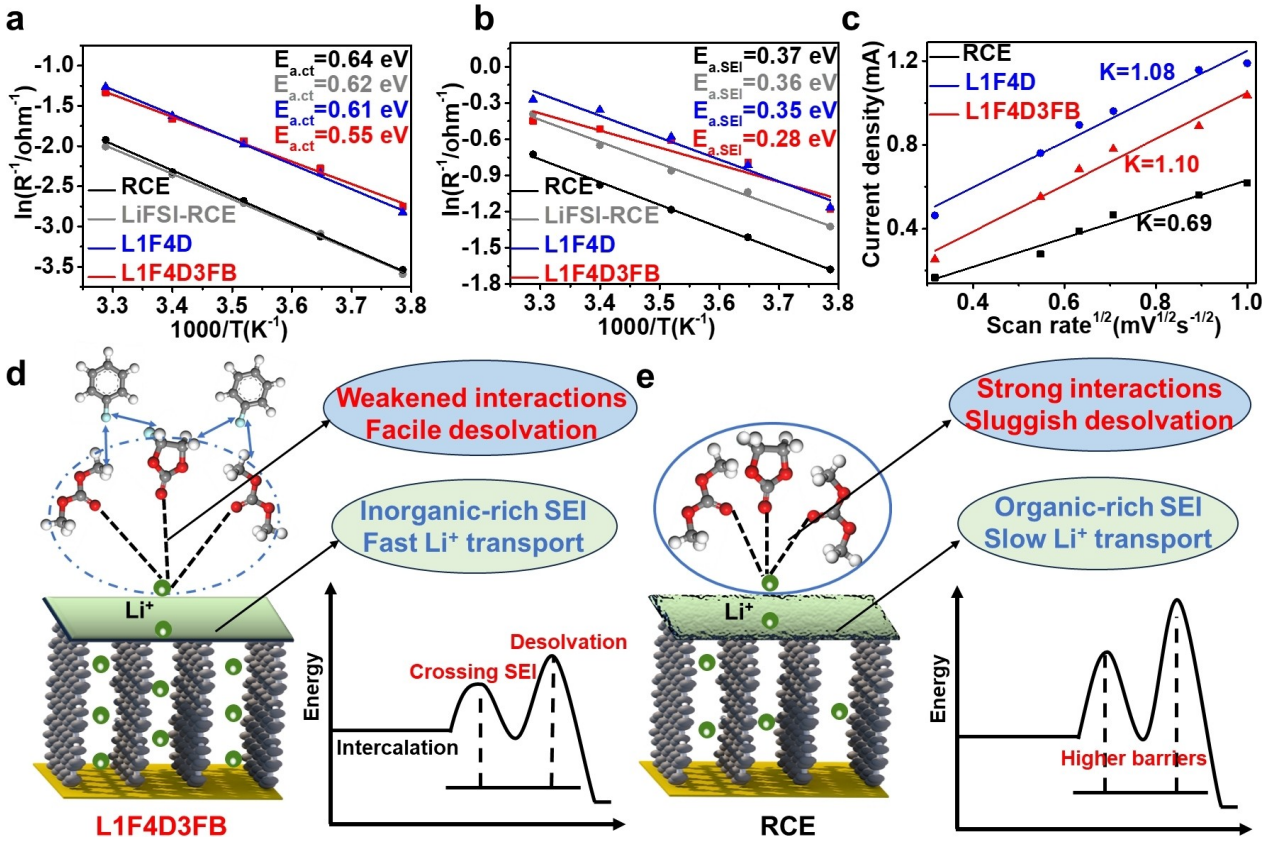

Figure 5. Kinetics of interfacial processes at the graphite/electrolytes interface measured by EIS and multistep CV. The activation energy for (a) charge transfer and (b) Li^+ transport through SEI in different electrolytes. (c) Determination of k value from the linear fitting. The energy diagram combined schematic diagram of interfacial processes for (d) L1F4D3FB and (e) RCE.

High-Rate and Low-Temperature Performance

Furthermore, we studied the interfacial compatibility towards high-nickel cathode (NCM622). Notably, the remarkable rate performance is observed in the NCM622/Li half cells using L1F4D3FB, revealing a substantial enhancement in rate capability of nickel-rich NCM (Figure 6a). The cells in L1F4D3FB and RCE show similar cycling stability (Figure 6b). To verify the applicability of L1F4D3FB, the NCM622/graphite pouch cell is assembled (Figure 6c). The cell demonstrates outstanding rate and cycling performance, retaining its capacity of 75% after 350 cycles at 1 C. By contrast, the pouch cell employing RCE delivers an inferior capacity retention and exhibits rapid capacity decay in the subsequent long-term cycle, which is caused by the possible structural degradation after fluctuated rates (Figures 6d, e and Figure S13). Although L1F4D3FB shows lower ionic conductivity of 5.54 mS cm^{-1} at 20 °C compared to RCE, the better rate performance means that the rate-determining step is the interfacial kinetics (desolvation and transport through SEI process) rather than ionic conductivity.

In addition, the L1F4D3FB shows low-temperature adaptability. As shown in Figure 6f, L1F4D and L1F4D3FB keep liquid state at −40 °C after removal of high-melting EC. The DSC result confirms that the L1F4D3FB remains liquid from −40 °C to 160 °C, while RCE delivers two apparent endothermic peaks at −1.45 °C and −26.67 °C attributed to the initial freezing of EC and further internal crystallization (Figure 6g).[42] Hence, the L1F4D3FB shows a high ionic conductivity of 1.48 mS cm^{-1} at −40 °C. In addition, the low viscosity of FB leads to superior wettability as denoted by lower contact angle of 47.75° (Figure S14). As a result, the NCM622/graphite full cell in L1F4D3FB exhibits high specific capacity of 84 mA h g^{-1} 0.2 C at −20 °C (Figure 6h and Figure S15), indicating its suitability for low temperature application, while the cell using RCE is unable to operate because of the solidification of EC solvent.

Conclusions

In summary, we develop an EC-free electrolyte by introducing non-coordinating FB for LIBs featuring enhanced rate capability, low-temperature adaptability and improved cycling stability. We demonstrate that (i) the dipole-dipole interaction between FB and solvents weakens Li^+-solvents coordination and facilitates desolvation, (ii) the loose solvation structure induced by FB promotes the entry of more anions and derives inorganic-rich SEI, which is crucial for high rate capability. The designed electrolyte enables Li/graphite cells to achieve a high specific capacity of 257 mA h g^{-1} at 6 C. The NCM622/graphite pouch cells exhibit excellent rate performance and superior cycling

Research Article
doi.org/10.1002/batt.202400034
Chemistry Europe
European Chemical Societies Publishing

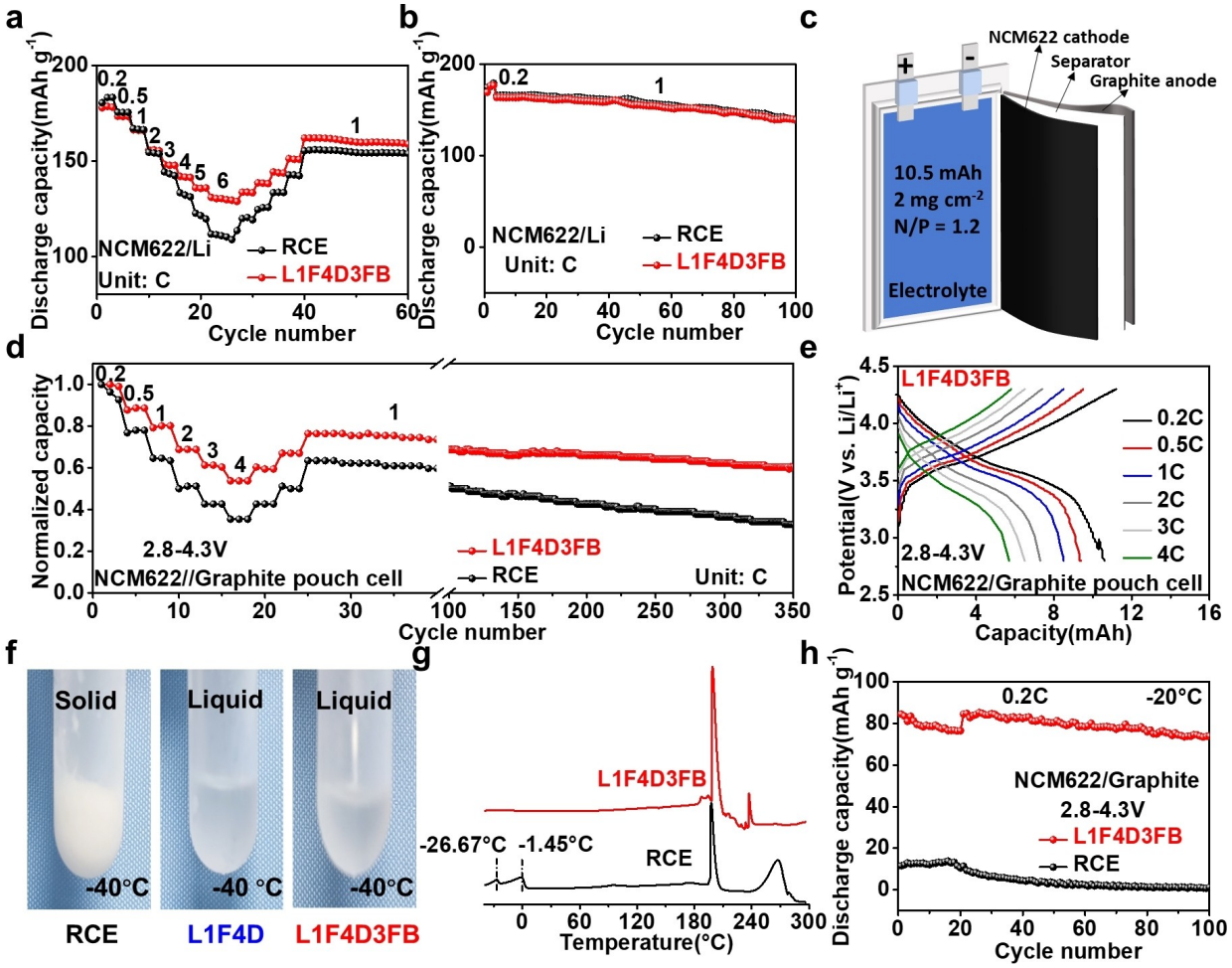

Figure 6. The rate capabilities and low-temperature application. (a) Rate performance and (b) cycling stability of NCM622/Li cells in varied electrolytes. (c) Designing parameters of pouch cell. (d) The rate performance of NCM622/graphite pouch cells in L1F4D3FB and RCE. (e) the corresponding charge-discharge curves. (f) Photographs of varied electrolytes at −40 °C. (g) DSC results of L1F4D3FB and RCE. (h) Cycling performance of NCM622/graphite cells in varied electrolytes at −20 °C.

capabilities (75% capacity retention after 350 cycles at 1 C). Even at −20 °C, the NCM622/graphite cells retain a specific capacity of 84 mA h g^{-1} at 0.2 C. The study offers an effective way to facilitate desolvation via dipole-dipole interaction in EC-free electrolyte and is expected to design high-rate LIBs.

Acknowledgements

This work was supported by the National Key Research and Development Program of China (No. 2022YFB2404800). The authors gratefully acknowledge the Analytical and Testing Center of HUST for allowing us to use their facilities. The authors thank Shiyanjia Lab (www.shiyanjia.com) and eceshi (www.eceshi.com) for helping with materials characterizations.

Conflict of Interests

The authors declare no conflict of interest.

Data Availability Statement

The data that support the findings of this study are available from the corresponding author upon reasonable request.

Keywords: Dipole-dipole interaction · fluorobenzene · desolvation · kinetics · lithium-ion batteries

[1] M. Qin, Z. Zeng, Q. Wu, X. Liu, Q. Liu, S. Cheng, J. Xie, *J. Energy Chem.* **2023**, *85*, 49–57.
[2] D. Larcher, J. M. Tarascon, *Nat. Chem.* **2015**, *7*, 19–29.
[3] W. Zhong, C. Zhang, S. W. Li, W. Zhang, Z. Q. Zeng, S. J. Cheng, J. Xie, *Sci. China Mater.* **2023**, *66*, 903–912.
[4] S. Li, H. Zhu, Y. Liu, Q. Wu, S. Cheng, J. Xie, *Adv. Mater.* **2023**, *35*, 2301967.
[5] G. G. Eshetu, H. Zhang, X. Judez, H. Adenusi, M. Armand, S. Passerini, E. Figgemeier, *Nat. Commun.* **2021**, *12*, 5459.
[6] L. Peng, C. Yu, S. Cheng, J. Xie, *Batteries & Supercaps* **2023**, *6*, e202200553.
[7] G.-L. Zhu, C.-Z. Zhao, J.-Q. Huang, C. He, J. Zhang, S. Chen, L. Xu, H. Yuan, Q. Zhang, *Small* **2019**, *15*, 1805389.

[8] M. Weiss, R. Ruess, J. Kasnatscheew, Y. Levartovsky, N. R. Levy, P. Minnmann, L. Stolz, T. Waldmann, M. Wohlfahrt-Mehrens, D. Aurbach, M. Winter, Y. Ein-Eli, J. Janek, *Adv. Energy Mater.* **2021**, *11*, 2101126.
[9] Y. Tao, C. D. Rahn, L. A. Archer, F. You, *Sci. Adv.* **2021**, *7*, eabi7633.
[10] M. Tesemma, F.-M. Wang, A. M. Haregewoin, N. L. Hamidah, P. Muhammad Hendra, S. D. Lin, C.-S. Chern, Q.-T. Pham, C.-H. Su, *ACS Sustainable Chem. Eng.* **2019**, *7*, 6640–6653.
[11] K. Xu, *Nat. Energy* **2021**, *6*, 763–763.
[12] M. Qin, Z. Zeng, X. Liu, Y. Wu, R. He, W. Zhong, S. Cheng, J. Xie, *Adv. Sci.* **2023**, *10*, 2206648.
[13] X. Fan, X. Ji, L. Chen, J. Chen, T. Deng, F. Han, J. Yue, N. Piao, R. Wang, X. Zhou, X. Xiao, L. Chen, C. Wang, *Nat. Energy* **2019**, *4*, 882–890.
[14] J. He, J. Meng, Y. Huang, *J. Power Sources* **2023**, *570*, 232965.
[15] Z. Wang, H. Wang, S. Qi, D. Wu, J. Huang, X. Li, C. Wang, J. Ma, *EcoMat* **2022**, *4*, e12200.
[16] Q. Li, Z. Cao, W. Wahyudi, G. Liu, G.-T. Park, L. Cavallo, T. D. Anthopoulos, L. Wang, Y.-K. Sun, H. N. Alshareef, J. Ming, *ACS Energy Lett.* **2021**, *6*, 69–78.
[17] W. Cai, Y.-X. Yao, G.-L. Zhu, C. Yan, L.-L. Jiang, C. He, J.-Q. Huang, Q. Zhang, *Chem. Soc. Rev.* **2020**, *49*, 3806–3833.
[18] M.-T. F. Rodrigues, G. Babu, H. Gullapalli, K. Kalaga, F. N. Sayed, K. Kato, J. Joyner, P. M. Ajayan, *Nat. Energy* **2017**, *2*, 17108.
[19] X. Zheng, Z. Gu, J. Fu, H. Wang, X. Ye, L. Huang, X. Liu, X. Wu, W. Luo, Y. Huang, *Energy Environ. Sci.* **2021**, *14*, 4936–4947.
[20] T. R. Jow, S. A. Delp, J. L. Allen, J.-P. Jones, M. C. Smart, *J. Electrochem. Soc.* **2018**, *165*, A361.
[21] Y. Yamada, M. Yaegashi, T. Abe, A. Yamada, *Chem. Commun.* **2013**, *49*, 11194–11196.
[22] L.-L. Jiang, C. Yan, Y.-X. Yao, W. Cai, J.-Q. Huang, Q. Zhang, *Angew. Chem. Int. Ed.* **2021**, *60*, 3402–3406.
[23] Y. Li, Y. Qi, *Energy Environ. Sci.* **2019**, *12*, 1286–1295.
[24] X. Zhang, L. Zou, Y. Xu, X. Cao, M. H. Engelhard, B. E. Matthews, L. Zhong, H. Wu, H. Jia, X. Ren, P. Gao, Z. Chen, Y. Qin, C. Kompella, B. W. Arey, J. Li, D. Wang, C. Wang, J.-G. Zhang, W. Xu, *Adv. Energy Mater.* **2020**, *10*, 2000368.
[25] J. Wang, Q. Zheng, M. Fang, S. Ko, Y. Yamada, A. Yamada, *Adv. Sci.* **2021**, *8*, 2101646.
[26] G. Åvall, J. Wallenstein, G. Cheng, K. L. Gering, P. Johansson, D. P. Abraham, *J. Electrochem. Soc.* **2021**, *168*, 050521.
[27] Y.-X. Yao, X. Chen, C. Yan, X.-Q. Zhang, W.-L. Cai, J.-Q. Huang, Q. Zhang, *Angew. Chem. Int. Ed.* **2021**, *60*, 4090–4097.
[28] T. Ma, Y. Ni, Q. Wang, W. Zhang, S. Jin, S. Zheng, X. Yang, Y. Hou, Z. Tao, J. Chen, *Angew. Chem. Int. Ed.* **2022**, *61*, e202207927.
[29] M. Qin, M. Liu, Z. Zeng, Q. Wu, Y. Wu, H. Zhang, S. Lei, S. Cheng, J. Xie, *Adv. Energy Mater.* **2022**, *12*, 2201801.
[30] H. Zhang, Z. Zeng, M. Liu, F. Ma, M. Qin, X. Wang, Y. Wu, S. Lei, S. Cheng, J. Xie, *Chem. Sci.* **2023**, *14*, 2745–2754.
[31] M. Qin, Z. Zeng, Q. Wu, H. Yan, M. Liu, Y. Wu, H. Zhang, S. Lei, S. Cheng, J. Xie, *Energy Environ. Sci.* **2023**, *16*, 546–556.
[32] M. Liu, X. Li, B. Zhai, Z. Zeng, W. Hu, S. Lei, H. Zhang, S. Cheng, J. Xie, *Batteries & Supercaps* **2022**, *5*, e202100407.
[33] D. Ouyang, K. Wang, Y. Pang, Z. Wang, *ACS Appl. Energ. Mater.* **2023**, *6*, 2063–2071.
[34] B. Umesh, P. Chandra Rath, R. F. H. Hernandha, J.-Y. Lin, S. B. Majumder, Q.-F. Dong, J.-K. Chang, *ACS Sustainable Chem. Eng.* **2020**, *8*, 16252–16261.
[35] H. B. Son, M.-Y. Jeong, J.-G. Han, K. Kim, K. H. Kim, K.-M. Jeong, N.-S. Choi, *J. Power Sources* **2018**, *400*, 147–156.
[36] D. Aurbach, Y. Ein-Eli, *J. Electrochem. Soc.* **1995**, *142*, 1746–1752.
[37] I. H. Cho, S. S. Kim, S. C. Shin, N. S. Choi, *Electrochem. Solid-State Lett.* **2010**, *13*, A168-A172.
[38] Y. Qi, S. J. Harris, *J. Electrochem. Soc.* **2010**, *157*, A741–A747.
[39] A. Shellikeri, V. Watson, D. Adams, E. E. Kalu, J. A. Read, T. R. Jow, J. S. Zheng, J. P. Zheng, *J. Electrochem. Soc.* **2017**, *164*, A3914–A3924.
[40] K. Xu, A. von Cresce, U. Lee, *Langmuir* **2010**, *26*, 11538–11543.
[41] M. Qin, W. Ren, R. Jiang, Q. Li, X. Yao, S. Wang, Y. You, L. Mai, *ACS Appl. Mater. Interfaces* **2021**, *13*, 3999–4007.
[42] Y.-G. Cho, M. Li, J. Holoubek, W. Li, Y. Yin, Y. S. Meng, Z. Chen, *ACS Energy Lett.* **2021**, *6*, 2016–2023.

Manuscript received: January 18, 2024
Revised manuscript received: February 23, 2024
Accepted manuscript online: February 26, 2024
Version of record online: March 11, 2024